Optical Studies of a Bacterial Photoreceptor Protein, Photoactive Yellow Protein, in Single Crystals†

Kingman Ng,‡,§ Elizabeth D. Getzoff,‖ and Keith Moffat*,‡

Department of Biochemistry and Molecular Biology, The University of Chicago, 920 East 58th Street, Chicago, Illinois 60637, and Department of Molecular Biology, The Scripps Research Institute, 10666 North Torrey Pines Road, La Jolla, California 92037

Received September 12, 1994; Revised Manuscript Received November 3, 1994⊗

ABSTRACT: Photoactive yellow protein (PYP), isolated from *Ectothiorhodospira halophila*, is a water soluble, 14 kDa photoreceptor protein with a fully reversible photocycle resembling that of sensory rhodopsin II. We have established the presence of photoactivity in PYP crystals and defined the relaxation kinetics of spectroscopically distinguishable species in quantitative terms. The PYP crystal has a bright yellow color and displays pronounced anisotropic absorption properties. Linear dichroism measurements show that the transition moment of the PYP chromophore makes an angle of 73° (or 107°) with respect to the six-fold crystallographic symmetry axis. The crystal absorbance can be bleached reversibly as indicated by absorption changes. A bleached photostationary state in the crystal can be established via CW laser illumination, and the extent of crystal bleaching is found to be clearly dependent on excitation laser wavelength, intensity and illumination time. These results provide the information for designing time-resolved crystallography experiments in which a minimum perturbation is applied to the PYP crystals. Global exponential fitting shows that the relaxation from the photostationary state in the crystal is biphasic at −4 °C; a slower component of 1.4 ± 0.2 s^{-1} accounts for 60% of the absorbance change and a faster component of 5.2 ± 0.9 s^{-1} for the other 40%. As a control, we found that the kinetics for the same relaxation in solution are well described by one exponential and agree quantitatively with previous studies. The two rate constants observed in the crystal show similar temperature dependences, with activation energies for the slow and fast components of 11.7 ± 1.2 and 5.5 ± 2.3 kcal/mol, respectively. However, the amplitudes associated with the two exponents show different and opposite temperature dependence. Our results show that the solution kinetic model is not directly applicable to crystals. A kinetic model consistent with the optical data is important to extract the underlying structural intermediates from the time-resolved X-ray diffraction data obtained in parallel with the optical data described here. We propose an alternative model for the photocycle in the crystal which contains an additional bleached intermediate in parallel with the last long-lived intermediate in the solution model.

Photoactive yellow protein (PYP)[1] from *Ectothiorhodospira halophila* is a small water soluble globular protein of 14 kDa with a distinct bright yellow color (Meyer, 1985). *E. halophila* is negatively phototactic, and the action spectrum of this photoresponse is similar to the absorption spectrum of PYP (Sprenger et al., 1993). PYP may therefore be a simple bacterial photosensor that binds a small chromophore and interacts with a secondary receptor in transduction of a light signal. Absorption of light by PYP initiates a fully reversible photocycle containing a series of discrete intermediates, each defined by a different optical absorption maximum (Meyer et al., 1987). The spectral intermediates presumably also differ in their tertiary structures, in a manner necessary for recognition and/or interaction with other receptor molecules (McRee et al., 1986; 1989). The light reaction of PYP is efficient enough to be biologically significant. The quantum yield for the formation of the final photoproduct is 0.64, as compared to 0.25 for the bacteriorhodopsin bR → M transformation at room temperature (Meyer et al., 1989). According to the kinetic model determined in solution as shown in Figure 1, the light induced photocycle of PYP shows initial rapid bleach of the yellow color ($k = 7.5 \times 10^3$ s^{-1}) followed by a slower dark recovery ($k = 2.6$ s^{-1}) (Meyer et al., 1989). The dark recovery step is slowed in the presence of glycerol and sucrose, which is presumed to be due to the viscous effects (Meyer et al., 1989) on changes in protein tertiary structure during the photocycle. Further evidence for such changes is provided by the presence of transient proton uptake and release during the photocycle (Meyer et al., 1993). The initial crystal structure of PYP (McRee et al., 1989) showed simple secondary structural elements and protein loops enfolding a small chromophore. The structure of the protein has very recently been reexamined and refined at 1.4 Å resolution (G.E.O. Borgstahl & E.D. Getzoff, personal communication). The chromophore is covalently linked to the protein at Cys 69 (Van Beeumen et al., 1993; Baca et al., 1994).

Complete elucidation of the mechanism of photobleaching requires both kinetic and structural information. It is difficult to determine unambiguously the relation of optical changes

† This work is supported by grants from the National Institutes of Health (GM36452 to K.M. and GM37684 to E.D.G.) and the W. M. Keck Foundation.

* To whom correspondence should be addressed.

‡ University of Chicago.

§ Present address: Division of Chemistry & Chemical Engineering 210-41, California Institute of Technology, Pasadena, CA 91125.

‖ The Scripps Research Institute.

⊗ Abstract published in *Advance ACS Abstracts,* December 15, 1994.

[1] Abbreviations: PYP, photoactive yellow protein; OD, optical density.

0006-2960/95/0434-879$09.00/0

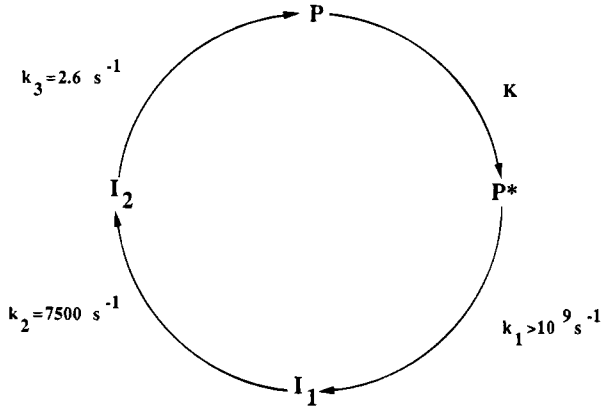

FIGURE 1: The photoactive yellow protein (PYP) bleaching and recoloring photocycle determined by laser flash photolysis at room temperature, with $k_1 > 10^9$ s^{-1}, $k_2 = 7500$ s^{-1}, and $k_3 = 2.6$ s^{-1} (Meyer et al., 1989).

to structural changes in most cases. High resolution structural information on proteins comes almost exclusively from conventional X-ray diffraction studies where the structure is averaged over a long time needed for data collection, much longer than the lifetimes of structural intermediates. However, recent advances in the Laue X-ray diffraction technique using intense synchrotron X-ray sources have demonstrated the feasibility of time-resolved structural studies of intermediates in biochemical reactions (Moffat, 1989; Cruickshank et al. (1992) and references therein; Hajdu & Andersson, 1993).

In order to understand the structural bases of photocycling and signal transduction in PYP, we have initiated a time-resolved crystallography study. The lifetimes of all intermediates are much shorter than 1 s and therefore present an unusual challenge to study. All previous time-resolved crystallographic studies involved much slower reactions in which the lifetimes of structural intermediates are minutes or tens of minutes (e.g. Schlichting et al., 1990; Singer et al., 1993). With this important exception, PYP appears to be well suited for time-resolved crystallography. The individual first order rate constants of the photocycle in solution (Figure 1) are quite different so there are time windows when the concentration of each intermediate is very high (see Figure 4 of Moffat et al., 1992). Reaction initiation which is both uniform throughout the crystal and rapid with respect to the subsequent reactions can be achieved by laser stimulation. As we will demonstrate, this requires careful experimental design; successful reaction initiation is one of the most difficult aspects of time-resolved crystallography to execute satisfactorily. The crystals belong to the high symmetry, hexagonal space group $P6_3$ with moderate unit cell dimensions, contain one molecule per asymmetric unit, diffract to high resolution (1.4 Å) (McRee et al., 1986), and are resistant to radiation damage arising from both X-ray and laser stimulation. These features make Laue data collection of PYP crystals very efficient and keep the spatial overlap problem in Laue diffraction (Cruickshank et al., 1991) to a minimum.

The activity of the protein in the crystal needs to be established and quantitated by optical or other means before attempting a time-resolved crystallography experiment. It is perhaps surprising that only a few macromolecules have had their activity in the crystalline state characterized in detail (Makinen & Fink, 1977; Mozzarelli et al., 1991; Hajdu & Andersson, 1993). Most functional and kinetic studies of proteins are carried out in dilute solution or under solvent conditions very different from those used for crystallization. The different solution conditions in the crystal and the structural restraints imposed by the intermolecular contacts in the crystal lattice may alter the kinetic behavior. Optical or other monitoring of crystals is necessary, but not sufficient; there may well be protein structural rearrangements which are not directly detected by these monitoring techniques. It is therefore particularly important also to be able to obtain simultaneous, time-resolved, kinetic, and structural data on the protein conformation. However, the two different crystal monitoring techniques, optical and crystallographic, have very different criteria for good data quality. The protein concentration in the PYP crystal is fixed and very high, 63 mM, and the extinction coefficient at the absorption maximum at 446 nm in solution is high, 45.5 mM^{-1} cm^{-1} (Meyer et al., 1989). The extinction coefficient in the crystal is also high as we demonstrate below. Thus, large crystals of dimensions of a few hundred micrometers suitable for X-ray analysis have an extremely high optical density (OD) at the wavelength of the absorption maximum. If stimulated at this wavelength, there would be highly nonuniform reaction initiation across the crystal. Most of the molecules at the front of the crystal nearest the laser source would indeed be stimulated and enter the photocycle, but those molecules in the interior and at the back would experience much lower light intensity and thus only a small fraction would be stimulated. Both a photochemical and a thermal gradient would be established across the crystal. The first confounds the X-ray analysis and the second causes the crystal to deform (Chen, 1994) which greatly increases the mosaic spread and reduces the quality of the X-ray diffraction pattern. Reaction monitoring is also hindered in large crystals, since large ODs cannot be accurately measured and the time course of the changes in OD may contain artifacts. Thus, successful laser reaction initiation and optical monitoring requires smaller crystals. On the other hand, the larger the crystal, the better the quality of X-ray data, the shorter the required X-ray exposure, and thus the better the time resolution that can be obtained.

In this paper, we describe the reaction initiation and optical monitoring aspects of time-resolved studies of PYP single crystals; the crystallographic aspects will be reported elsewhere (manuscripts in preparation). Crystal optical properties can be studied off-line in subsidiary experiments or on-line during X-ray crystallographic data collection. We demonstrate how to establish quantitatively a photostationary state in PYP crystals and to monitor decay from the photostationary state to the dark, ground state. Such results are essential for the design of associated time-resolved crystallography experiments. We consider possible kinetic models for the photocycle in the PYP crystal and how these data may aid in extracting structural intermediates from the crystallographic data. Although our theory and results deal directly with PYP, they illustrate general principles of light-initiated and light-monitored crystallographic experiments and as such are applicable to many types of crystals.

MATERIALS AND METHODS

Protein Preparation and Crystallization. PYP was purified by D. R. Williams and P. M. Burke of The Scripps Research Institute from *E. halophila* strain BN9626 as

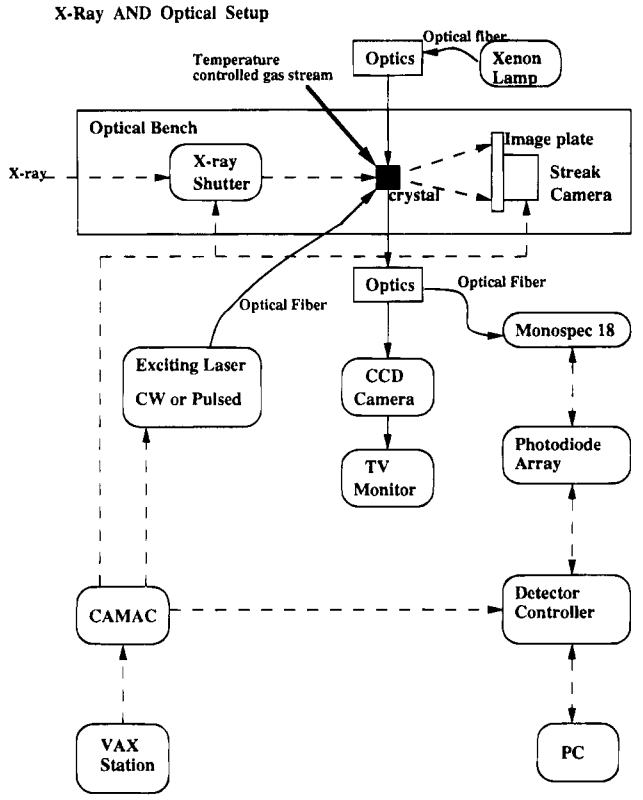

FIGURE 2: Block diagram of X-ray and optical apparatus for time-resolved crystallography (Moffat et al., 1992).

described before (Meyer, 1985). Crystals were grown by vapor diffusion against 68% saturated ammonium sulfate at pH 7.0 (McRee et al., 1986). All crystals were grown by G.E.O. Borgstahl, D. R. Williams, P. M. Burke, and C.-F. Kuo of The Scripps Research Institute. The crystals are hexagonal in cross section and usually taper to a point at one end; they resemble tiny pencils. They belong to the space group $P6_3$ with $a = b = 66.9$, $c = 40.8$ Å with one molecule per asymmetric unit (McRee et al., 1986).

Microspectrophotometric Measurements. Static absorption spectra and linear dichroism measurements were carried out on a microspectrophotometer designed and built around a high performance microscope (Leitz Ortholus I). The details of this instrument are described elsewhere (Churg & Makinen, 1978; Zelano et al., 1985). Very tiny crystals of size $0.1 \times 0.02 \times 0.03$ mm^3 or smaller were used for these measurements. Typically, the crystal was placed in a drop of mother liquor and sealed between two cover slips.

Time-resolved on-line and off-line optical monitoring experiments were carried out with a microspectrophotometer assembled around a Laue bench X-ray camera as shown in Figure 2. The design and performance of the microspectrophotometer have been described elsewhere (Chen et al., 1994). The crystal was mounted in a 0.7 mm or 1.0 mm diameter capillary. The typical crystal size used for on-line X-ray and optical monitoring was $0.25 \times 0.05 \times 0.03$ mm^3. Temperature control was achieved by directly blowing dry air over the capillary, where the air temperature was controlled by a commercial crystal cooler (FTS Systems). The excitation light to establish the photostationary state was provided by a CW argon ion laser (Coherent Innova 70). The laser beam was focused and coupled into a multimode optical fiber via an optical fiber coupler (Oz Optics). Typically, 80% coupling efficiency is accomplished because the laser beam has a small beam diameter and low beam divergence. The output of the fiber was focused with another lens onto the crystal and was delivered at an angle of about 45° to the measuring light. The diameter of the focused beam was about 0.8 mm (full width at half maximum) and was deliberately made much larger than the maximum crystal dimension, to minimize transverse gradients of optical illumination. With this broad focus, the incident intensity varies by less than 15% across the entry face of a 0.25 mm long crystal. In contrast to the exciting beam, the monitoring beam has to be much smaller than the crystal size. There is no adjustable diaphragm in our microspectrophotometer design, and the monitored area of the crystal is determined by the size of the measuring light beam. The measuring beam diameter can be adjusted between 0.015 and 0.05 mm (full width at one-tenth maximum), and we typically used values around 0.025 mm.

Optical Experimental Design. A typical optical experiment is carried out in the following sequence. The photocycle is initiated by continuous laser stimulation to establish the photostationary state in the crystal. The timing of the experiment was set by a home built, six-channel, programmable time module/pulse train generator (SCT 7513), which provided trigger pulses for the laser shutter and photodiode array detector controller. The timing module SCT 7513 was in turn activated via a CAMAC module controlled by IDL programs running on a DEC VAX station. The laser shutter was first opened for 200 ms with typical power around 100 mW mm^{-2}. When the laser shutter was closed, a trigger pulse was sent to the diode array detector to initiate optical data acquisition. The total data acquistion time was set by the total number of spectra times the exposure time used for each spectrum, both of which were adjustable by the detector controller software OSMA (Princeton Instruments) running on a PC.

Kinetic Data Analysis. Kinetic analysis of the optical data using global exponential fitting performed with PC-Matlab (The MathWorks, South Natick, MA). Some further calculations and plotting were performed with SigmaPlot (Jandel Scientific, San Rafael, CA).

An optical data file typically consists of spectra which were recorded sequentially at different time delays after the laser was shut off. Each spectrum has 512 data points, one for each diode; they are transmission spectra in which counts are proportional to the light intensity transmitted through the crystal. The 512 diode array corresponds to a wavelength range of 385−525 nm. Background was first subtracted from the measured transmission spectra. The absorbance difference was calculated as the logarithm of the ratio of the background-corrected transmission spectra to the final spectrum in a data set which corresponded to the dark or ground state. The resulting set of difference spectra is in the form of a matrix $\mathbf{D}$ $(m \times n)$ and can then be subjected to kinetic analysis. The parameter m corresponds to the 512 wavelengths at which measurements were made for one spectrum. The parameter n is the number of spectra collected in a time-resolved data set. We select m' wavelengths ($m' < m$) with good signal to noise level at wavelengths which are distant from the absorption peak, where the OD is extremely high. As a result, $\mathbf{D}$ $(m \times n)$ is now reduced to $\mathbf{D}'$ $(m' \times n)$. We rewrite $\mathbf{D}'$ $(m' \times n)$ as follows:

$$\mathbf{D}'(m' \times n) = \mathbf{A}(m' \times p)\mathbf{K}(p \times 1)\mathbf{t}(1 \times n)$$

where $\mathbf{t}(1 \times n)$ is a time point matrix, and p is the number of exponentials used for fitting the kinetic data. $\mathbf{K}$ is an operator and can be explicitly written as

$$\mathbf{K} = \begin{pmatrix} \exp(-k_1) \\ \exp(-k_2) \\ \exp(-k_3) \end{pmatrix}$$

if three exponentials are used for fitting. $\mathbf{A}$ $(m' \times n)$ is the coefficient or amplitude matrix for the exponential components at each of the m' selected wavelengths. The optimal solution of $\mathbf{A}$ and the values of k_i in $\mathbf{K}$ are obtained by the nonlinear least squares Levenberg–Marquardt method using the Matlab optimization toolbox (The MathWorks Inc.). Errors in the parameters were obtained from the covariance matrix.

RESULTS

Optical Properties of PYP Crystals. We performed plane-polarized absorption measurements of single PYP crystals at room temperature in order to examine their optical anisotropy. The appropriate orientation of the crystal with respect to the optic axis of the microscope was first determined by linear birefringence measurements. We observed linear birefringence with the long axis of the PYP crystal perpendicular to the optic axis of the microscope. The long axis of the crystal contains the six-fold crystallographic axis of symmetry. As a control, a crushed polycrystalline slurry did not show any birefringence. Two axes can be defined from the birefringence measurements, one parallel and one perpendicular to the crystal long axis. Due to the PYP crystal morphology, it is not possible to measure the absorption along the crystal long axis. The two plane polarized absorption spectra of the PYP crystal at room temperature are characterized by a single peak at 449 nm (Figure 3). The crystal spectrum is very similar in shape to the solution spectrum with the peak position red-shifted by 3 nm in the crystal.

A salient feature of the PYP crystal spectrum is the large difference between absorbance measured with the plane of polarization parallel or perpendicular to the crystal long axis. The absorption of the crystals could therefore be greatly reduced by controlling the orientation of the plane of polarization with respect to the crystal axes. The polarization ratio is defined as the ratio of the optical density measured with plane-polarized light in which the plane of polarization contains the six-fold long axis of the crystal (parallel) to that in which the plane of polarization is perpendicular to this axis. The polarization ratio generally depends solely on the orientation of the transition dipole of the chromophore with respect to the crystal axes. Figure 4 shows the PYP polarization ratio versus wavelength. The ratio is constant at 0.19 ± 0.01 in the wavelength range of 400–470 nm, which indicates that the transition moment corresponding to the absorption band can be characterized by a single polarization direction. Thus, without knowing the detailed molecular structure of the chromophore, the simplest model for the PYP chromophore is a single transition polarized parallel to a molecular direction z defined by a Cartesian coordinate with the extinction coefficient ϵ_z. The orientation of the molecular z axis with respect to the axes $(a\ b\ c)$ is specified by the direction cosines $\cos(za)$, $\cos(zb)$, and

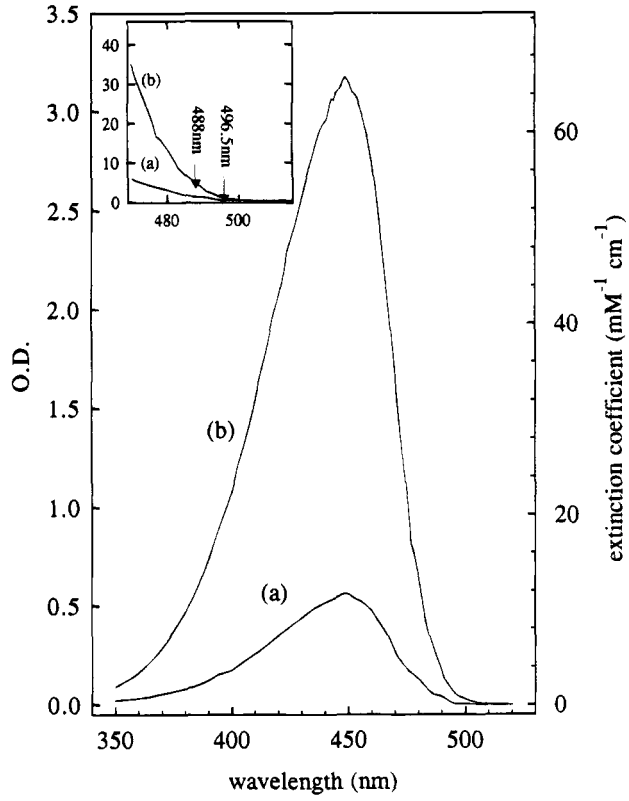

FIGURE 3: Plane polarized absorption spectra of the PYP crystal at room temperature. (a) Monitoring light with the plane of polarization parallel to the crystal long axis, which contains the six-fold crystallographic axis of symmetry. (b) Monitoring light with the plane of polarization perpendicular to the crystal long axis. The spectra are plotted with the measured optical density (OD) values. The extinction coefficients are calculated with a simple model for the transition moment for the PYP chromophore in the crystal lattice and its orientation deduced from the polarization ratio. The inset shows the extinction coefficients (in mM^{-1} cm^{-1}) for the two polarization directions in the long wavelength tail end of the absorption spectrum. The two arrows indicate the two laser lines of an argon ion laser, which are used for photoinitiation.

$\cos(zc)$, where $\cos^2(za) + \cos^2(zb) + \cos^2(zc) = 1$. This condition only holds for orthogonal axes whereas the PYP crystal axes are not orthogonal. We retain the crystallographic c axis and define two orthogonal axes a' and b' in the plane perpendicular to c. The projections of the molecular extinction coefficient on to the axes $(a'\ b'\ c)$ are given by

$$\epsilon_{a'} = \epsilon_z \cos^2(za'); \epsilon_{b'} = \epsilon_z \cos^2(zb'); \epsilon_{c'} = \epsilon_z \cos^2(zc) \quad (1)$$

Since c is the crystal axis of symmetry, a' and b' are identical and we have $\epsilon_{a'} = \epsilon_{b'}$. Thus,

$$\epsilon_{a'} + \epsilon_{b'} = \epsilon_z(\cos^2(za') + \cos^2(zb')) \quad (2)$$

and

$$\epsilon_{a'} = \frac{\epsilon_z(1 - \cos^2(zc))}{2} = \frac{\epsilon_z \sin^2(zc)}{2} \quad (3)$$

The polarization ratio is then given by

$$r = \frac{\epsilon_{c'}}{\epsilon_{a'}} = \frac{2\cos^2(zc)}{\sin^2(zc)} = 2\cot^2(zc) \quad (4)$$

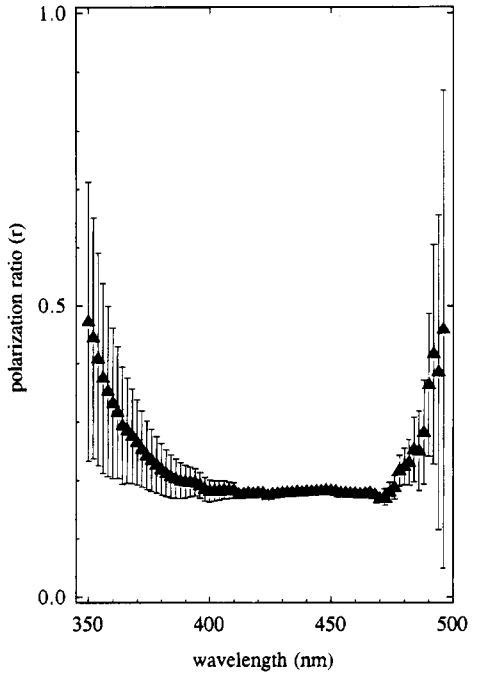

FIGURE 4: The polarization ratio (r) as a function of wavelength from 350 to 500 nm for the PYP crystal measured at room temperature. Error bars are also shown; the values of r are both precise and constant in the wavelength range of 400−470 nm.

The transition polarization direction or the molecular z direction (according to our notation) can then be calculated to make an angle of either 73.0 ± 0.1° or 107.0 ± 0.1° with the crystal $+c$ axis. The first chromophore orientation in the crystal is supported by recent crystallographic results (G.E.O. Borgstahl & E.D. Getzoff, personal communication).

For an ideal "oriented gas" where the chromophore orientation is fixed in space with no interactions among the chromophores, an isotropic extinction coefficient ϵ_i can be defined as $\epsilon_i = {}^1/_3(\epsilon_x + \epsilon_y + \epsilon_z)$. With our simple model for the PYP chromophore transition moment, $\epsilon_x = \epsilon_y = 0$; and ϵ_i can be assumed to be the same as the solution extinction coefficient. Thus $\epsilon_z = 3\epsilon_i$, and the extinction coefficients in the crystal for the parallel and perpendicular polarization can be calculated with the assumption that the absorption spectrum in crystal has the same shape as in solution and the extinction coefficient at 446 nm, the absorption peak is 45.5 mM^{-1} cm^{-1} (Meyer et al., 1989). As a result $\epsilon_\perp = \epsilon_{a'} = 0.46\epsilon_z$, and $\epsilon_{||} = \epsilon_c = 0.09\ \epsilon_z$. In this way the extinction coefficients of the PYP crystal are determined and are also shown in Figure 3. (Note that these values are only appropriate for low light levels, where no significant bleaching of the crystals occurs; see below).

Selection of Conditions for Uniform Reaction Initiation. PYP crystals have a very large absorbance in the visible blue region. This introduces potential problems in optical monitoring and reaction initiation by optical means. If the crystal is excited at a wavelength where the absorbance is very large, only the molecules within a small surface layer will be excited, as noted above. Therefore, careful selection of excitation conditions is necessary in order to obtain a uniform and complete photostationary state in the crystal. According to the model shown in Figure 1, the PYP photocycle lifetime is controlled by the last step ($k = 2.6\ s^{-1}$), and the bleached state I_2 has an absorption maximum below 370 nm (Meyer et al., 1987). For simplicity assume a two state system, P and I_2, and consider a wavelength for reaction initiation where only the dark state P absorbs but the bleached photoproduct I_2 does not. The time and spatial dependence of the bleached state can be described by the following differential equations:

$$dI(x,t) = -2.303[OD]I(x,t)[1 - R(x,t)]dx \qquad (5)$$

and

$$dR(x,t) = \{I(x,t)[1 - R(x,t)] - R(x,t)\}dt \qquad (6)$$

where $I(x,t)$ is the excitation light intensity and $R(x,t)$ is the extent of photobleaching in the crystal. Both are functions of time and position in the crystal. OD is the crystal optical density in the ground state defined by the extinction coefficients and crystal thickness using Beer's law. The variables I, t, and x are dimensionless, scaled by I_s, t_e, and x_o respectively. $t_e = 1/k_3$ is the lifetime of the bleached state and x_o is the total crystal thickness in the excitation beam direction. I_s is a characteristic intensity defined as:

$$I_s = \frac{N_A hck_3}{Q\epsilon\lambda}$$

where N_A is Avogadro's number, h is Planck's constant, c is the velocity of light, λ is the excitation light wavelength, ϵ is the extinction coefficient at that wavelength, k_3 is the first order rate constant for decay from I_2 to P, and Q is the quantum yield of photoactivation. Thus, I_s is wavelength-dependent. At steady state $dR/dt = 0$, and we have

$$\frac{1}{R(x)} = 1 + \frac{1}{I(x)} \qquad (7)$$

Combining eqs 5 and 7, we have

$$\frac{dI(x)}{dx} = \frac{-I(x)}{I(x) + 1}$$

and hence $I(x)$ at steady state is given by

$$\ln\left(\frac{I(x)}{I_o}\right) + [I(x) - I_o] = -2.303[OD]x \qquad (8)$$

where I_o is the incident excitation light intensity. Equation 7 shows that the extent of photobleaching R is dependent on I, and that 50% photobleaching is achieved at a depth x when the excitation light intensity at that depth is equal to I_s; eq 8 shows that the attenuation of I in the crystal is not governed by Beer's law.

As a result, careful selection of excitation conditions is necessary to achieve spatially uniform photobleaching inside the crystal in the photostationary state. If a very high excitation intensity is used, this increases R but causes undesirable thermal gradients in the crystal. There are two other experimentally accessible variables that affect the variation of R inside the crystal in the photostationary state: (1) excitation wavelength and its corresponding extinction coefficient; (2) crystal thickness. Figure 5 shows R in the photostationary state as a function of position in the crystal at a fixed incident excitation light intensity $I_o = I_s$. For case 1 when excitation at different wavelengths with different extinction coefficients is compared, Figure 5 shows clearly that the variation of R inside the crystal is largely dependent

on the extinction coefficient of the dark state P at the excitation wavelength. Consequently, the extent of photobleaching is much more spatially uniform across the crystal when the excitation wavelength is chosen to correspond to a smaller extinction coefficient. This suggests that uniform excitation can be readily achieved on the long wavelength end of the 449 nm band for PYP crystals, using for example argon ion laser lines at 488 or 496.5 nm. Since the exciting laser light from the optical fiber is unpolarized, the absorption at these two laser wavelengths by the crystal is determined by the isotropic extinction coefficients. These are calculated as described above to be 2.55 and 0.72 mM^{-1} cm^{-1} at 488 and 496.5 nm, respectively, and they generate OD values of 0.8 and 0.22 for a crystal of 0.05 mm thickness, which are still somewhat high. To minimize photochemical and thermal gradients, all time-resolved crystallographic experiments used unpolarized exciting light at 496.5 nm. The absorption could be further reduced by using a plane-polarized laser beam where the orientation of the plane of polarization with respect to the crystal axes is controlled. However, photoselection effects may prevent some molecules from being excited and we chose not to take advantage of this possibility.

For case 2, consider two excitation wavelengths at which the extinction coefficients differ by a factor of 10. With the lower extinction coefficient, doubling the crystal thickness and thereby increasing the OD from 0.1 to 0.2 reduces R by no more than 10%. With the higher extinction coefficient, increasing the OD from 1 to 2 reduces R very significantly inside the crystal (Figure 5). Clearly, excitation at a wavelength with a lower extinction coefficient is also much less sensitive to crystal size variations. Numerical calculations which describe the time dependence of excitation intensity and extent of photobleaching in the crystal when approaching the photostationary state have been presented elsewhere (Moffat et al., 1992; Chen, 1994).

Establishing a Photostationary State. The PYP photocycle kinetics have been determined in solution (Meyer et al., 1987, 1989). According to this model (Figure 1), the 446 nm band disappears and a new absorption maximum appears below 370 nm during the photocycle and thus is referred to as a bleaching reaction. The light-induced photocycle in solution shows nanosecond initial bleaching, followed by slower sub-millisecond dark bleaching with recovery of the yellow color on a subsecond time scale at room temperature. The time dependence of each intermediate can be described by the following set of differential equations:

$$\begin{aligned} (D + K)\mathrm{P} &= k_3\mathrm{I}_2 \\ (D + k_1)\mathrm{P}^* &= K\mathrm{P} \\ (D + k_2)\mathrm{I}_1 &= k_1\mathrm{P}^* \\ (D + k_3)\mathrm{I}_2 &= k_2\mathrm{I}_1 \\ \mathrm{P} + \mathrm{P}^* + \mathrm{I}_1 + \mathrm{I}_2 &= 1 \end{aligned} \tag{9}$$

where fractional concentrations are used, D is the operator d/dt and KP is the pumping rate and so is dependent on the excitation light intensity and the concentration of P. The formation and breakdown of P* probably only involves electronic transitions. Since PYP has a very low fluorescence

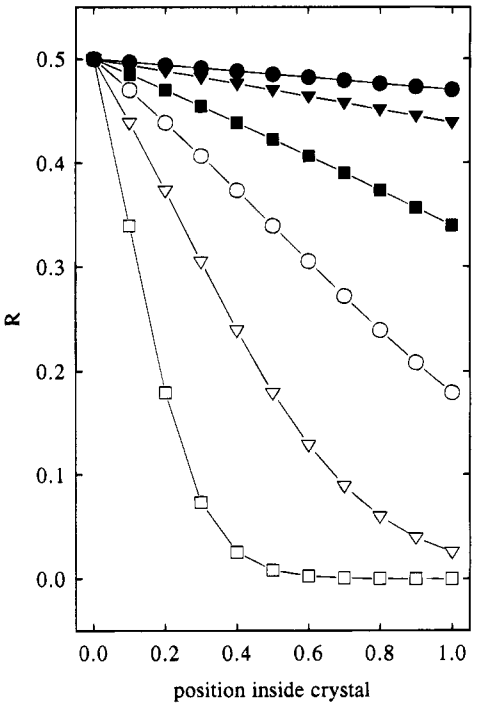

FIGURE 5: The effects of OD due to (1) excitation at different wavelengths with different extinction coefficients; (2) different crystal thickness, on the spatial extent of bleaching as a function of position in the crystal in the photostationary state. These curves are calculated using eqs 7 and 8 (see Results). An incident excitation light intensity of I_s at the front end of the crystal is used. Six cases of different ODs are plotted: (●) OD = 0.1; (▼) OD = 0.2; (■) OD = 0.5; (○) OD = 1.0; (△) OD = 2.0; (□) OD = 5.0.

quantum yield of 1.4×10^{-3} (Meyer et al., 1991), P* decays mainly via the route of the photocycle, which occurs on the sub-nanosecond time scale (Meyer et al., 1987) and is thus much too fast to be detected structurally. The step $\mathrm{I}_1 \rightarrow \mathrm{I}_2$ has a lifetime of about 100 μs. Structural monitoring of this step would require an X-ray exposure time around 10 μs and is barely feasible with today's synchrotron X-ray sources. However, the lifetime of the photocycle is controlled by the slow recovery of I_2 back to P with $k_3 = 2.6$ s^{-1} in solution (Meyer et al., 1989).

From eq 9, photostationary states in which $D\mathrm{P} = D\mathrm{P}^* = D\mathrm{I}_1 = D\mathrm{I}_2 = 0$ can be established for all values of $K > 0$. The following conditions then hold simultaneously in all photostationary states:

$$\mathrm{P}^* = \frac{K}{k_1}\mathrm{P};\quad \mathrm{I}_1 = \frac{K}{k_2}\mathrm{P};\quad \mathrm{I}_2 = \frac{K}{k_3}\mathrm{P} \tag{10}$$

With the rate constants $k_1 \geq 10^9$ s^{-1}, $k_2 = 7.5 \times 10^3$ s^{-1} and $k_3 = 2.6$ s^{-1} from the solution model, and with the assumption that $\mathrm{P} \rightarrow \mathrm{P}^*$ is the only light driven reaction of the PYP photocycle (Figure 1), the concentration of I_2 is very much larger than P* and I_1 at the photostationary state. Thus, the relative OD change reflects the extent of I_2 formation and is dependent on excitation laser intensity. The percentage of I_2 in photostationary state can be increased by gradually increasing K with higher excitation laser intensity. In order to obtain a saturated photostationary state in which the concentration of I_2 relative to P becomes saturated and cannot be increased further by higher laser intensity, the pumping rate must be much larger than the rate of return to the ground state. A bleached, saturated,

photostationary state can be readily established via continuous excitation with relatively low CW laser power and short laser illumination. The kinetics of relaxation back to the dark or ground state following interruption of the laser can then be monitored by optical and Laue techniques.

We have found the PYP crystal to undergo bleaching when excited at 488 or 496.5 nm but not at 514 nm where the crystal is completely transparent. We have also found that a saturated photostationary state is established on a subsecond time scale characterized by a steady OD difference. A difference spectrum is simply obtained by subtracting the OD observed with the exciting laser on from the OD measured with laser off. We define the relative OD change as follows:

$$f_{OD} = \frac{(OD_o - OD_s)}{OD_o} \tag{11}$$

where OD_o is the OD with laser off and OD_s is that in the photostationary state with the laser on.

Figure 6a shows the dependence of f_{OD} on total laser power. These values were measured at −4 °C with the plane of polarization of the monitoring beam parallel to the crystal long axis. The values of f_{OD} saturate as the laser power is increased with a fixed laser illumination time of 200 ms. Similar saturation was also observed as the laser exposure time was increased at a fixed laser power of ~100 mW mm^{-2}, as shown in Figure 6b. These results indicate that a saturated photostationary state in the crystal can be readily obtained, in qualitative agreement with the model, and establish the minimum laser power and exposure time necessary to achieve this state. This is essential for designing time-resolved crystallography experiments in order to keep thermal perturbations on the crystal to a minimum. The values of f_{OD} determined at the long wavelength end of the absorption band (with ODs smaller than 2.0) saturate at about 0.5 (Figure 6, parts a and b).

To convert the values of f_{OD} to the extent of photobleaching R, the true extinction coefficients of the intermediates in the PYP photocycle must be known. In general,

$$f_{OD} = \frac{\sum_i f_i(\epsilon(P) - \epsilon_i(I_i))}{\epsilon(P)} \tag{12}$$

where f_i is the fraction of the intermediate i with an extinction coefficient of $\epsilon(I_i)$, and $\epsilon(P)$ is the extinction coefficient for the ground state. We define an effective extinction coefficient $\epsilon(PS)$ for the photostationary state, and simplify eq 12 to

$$f_{OD} = R\left(1 - \frac{\epsilon(PS)}{\epsilon(P)}\right) \tag{13}$$

Since R cannot be greater than unity, we have from eq 13

$$R = f_{OD}\left(1 - \frac{\epsilon(PS)}{\epsilon(P)}\right)^{-1} < 1.0$$

and therefore,

$$\epsilon(PS) < [1 - f_{OD}]\epsilon(P)$$

If the measured saturation value of f_{OD} at 0.5 represents total bleaching, $\epsilon(PS)$ is 22.8 mM^{-1} cm^{-1}. Thus, our results indicate that the photostationary state still retains some absorption at the 446 nm peak. It is possible that the photostationary state is composed of a mixture of intermediates but their corresponding extinction coefficients have not been determined conclusively.

Photostationary State Relaxation. According to the model shown in Figure 1 and the set of differential eq 9, the relaxation from the photostationary state can be described by the following equations:

$$DP^* = -k_1P^*$$

$$DI_1 = -k_1P^* - k_2I_1$$

$$DI_2 = k_2I_1 - k_3I_2$$

where D is the operator d/dt. P*, I_1, and I_2 are fractional concentrations. These equations can be solved to give the time dependence of the fractional concentration of each intermediate:

$$P^*(t) = C_1e^{-k_1t}$$

$$I_1(t) = \frac{k_1C_1}{k_2 - k_1}\left(e^{-k_1t} - \frac{k_1}{k_2}e^{-k_2t}\right) \tag{14}$$

$$I_2(t) = \frac{k_1C_1}{k_2 - k_1}\left[\frac{k_2}{k_3 - k_1}e^{-k_1t} - \frac{k_1}{k_3 - k_2}e^{-k_2t} + \frac{k_1(k_3 - k_2)(k_1 - k_2 - k_3) + k_1k_3(k_3 - k_1)}{k_3(k_3 - k_1)(k_3 - k_2)}e^{-k_3t}\right]$$

where C_1 is a constant determined by initial conditions. The OD changes for species I_i as a function of time are related to the difference in extinction coefficients $\Delta\epsilon_i$ and are thus given by

$$\Delta OD_i = C_o\Delta\epsilon_iI_i(t)$$

where C_o is the total protein concentration in the sample and the values of $I_i(t)$ are given by eqs 14. As noted above, the relaxation from the photostationary state is practically given by the time course of I_2 or ΔOD_2 only, which is in the form of multiple exponentials:

$$I_2(t) = A_1e^{-k_1t} + A_2e^{-k_2t} + A_3e^{-k_3t}$$

where the amplitudes A_i are related to the exponents k_i by eq 14. According to the solution model (Figure 1), $k_1 \sim 10^9$ s^{-1}; $k_2 \sim 10^4$ s^{-1} and $k_3 \sim 10^0$ s^{-1}. With these rate constants, we have

$$\frac{A_1}{A_3} \approx 10^{-14}; \qquad \frac{A_2}{A_3} \approx 10^{-4}$$

Thus, the current model from solution studies predicts monophasic relaxation from the photostationary state with a rate constant of k_3.

Time-Resolved Optical Data Analysis. Figure 7 shows the difference spectrum obtained immediately after the exciting laser beam was interrupted. The OD change is positive below 400 nm, large and negative around 450 nm and drops to zero above 500 nm. This is closely similar to that

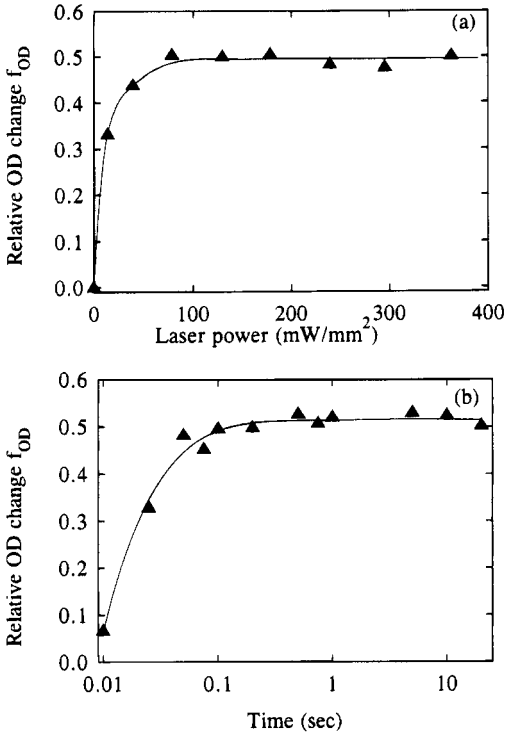

FIGURE 6: (a) The effects of CW laser power at 496.5 nm on the observed relative OD change. The measurements were made at −4 °C, with the plane of polarization of the monitoring light parallel to the crystal long axis. (b) The effects of CW laser illumination time on the observed relative OD change. The measurements were made at ~100 mW/mm^2 and −4 °C.

observed for I_2 in solution (see Figure 1 of Meyer et al., 1987), with some minor differences. The photostationary state in the crystal, as in solution, appears to have another absorption maximum below 400 nm as indicated by the positive ΔOD (Figure 7). However, the exact peak position cannot be determined as we cannot make reliable measurements below 380 nm with the present optical system. There is an isosbestic point at about 400 nm, which is red-shifted by about 20 nm relative to that obtained in solution (Meyer et al., 1987). The shoulder on the blue end of the peak is much more noisy than on the red end due to the weaker monitoring lamp spectrum and the lower diffraction grating efficiency below 425 nm. The very large and noisy ΔOD in the vicinity of 450 nm is due to the very large OD and these measurements between 410 and 465 nm are not sufficiently accurate for quantitative kinetic analysis.

We have applied global exponential fitting to analyze the optical data. Kinetic analysis was applied to optical densities at 20 selected wavelengths where the OD can be measured accurately at all time points, for example at 470 nm and above as shown in Figure 7. These analyses gave two exponential components. As a control, we have also determined the rates of relaxation from the photostationary state in solution (Table 1). The rates we obtain in solution at low ionic strength are closely similar to those of Meyer et al. (1989). It is important to note that we find the kinetics in solutions to be well described by a single exponential. This indicates that the present experimental and data analysis approaches do not contribute any major artifacts to the measured kinetics, and in particular, they do not generate a spurious second exponential. The two rate constants in solution with different salt conditions are also very similar, which again agrees with Meyer et al. (1987).

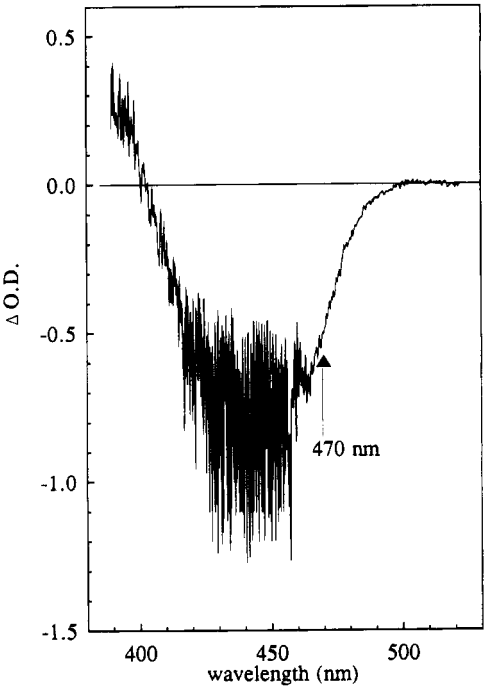

FIGURE 7: Difference spectrum for the PYP photostationary state. The experiments were carried out at −4 °C, with CW laser illumination at 496.5 nm for 200 ms. The spectrum is plotted in the form of ΔOD as a function of wavelength. Negative ΔOD values mean that the bleached photostationary state has less absorbance than that of the ground state, and vice versa. Due to the very high absorbance of the ground state around 450 nm, the difference spectrum is very noisy between 425 and 465 nm. The arrow points at 470 nm where data obtained at wavelengths above this point have much better signal to noise level.

Table 1: Comparison of Relaxation Rate Constants from the Photostationary State Measured in Crystals and in Solution with Different Solvent Conditions

1.5 s^{-1}	from Figure 3 of Meyer et al. (1989), 5 mM sodium phosphate, pH 7.0, 10 °C
2.85 ± 0.02 s^{-1}	this work, solution, 10 mM sodium phosphate, pH 7.0, 10 °C
2.75 ± 0.05 s^{-1}	this work, solution, 50% saturated ammonium sulfate, 10 °C
2.2 ± 0.4 s^{-1} [1.4 ± 0.2 s^{-1}/60%; 5.2 ± 0.9 s^{-1}/40%][a]	this work, crystal, −4 °C, on-line experiment carried out at synchrotron in June, 1993

[a] If two exponentials are used for fitting.

Temperature Dependence of Relaxation from the Photostationary State. Qualitatively, the rates of relaxation decrease when the temperature is decreased. Multiwavelength exponential fitting reveals clearly biphasic kinetics at some temperatures. The data at 470 nm obtained in the crystal at several different temperatures are shown in Figure 8a. Our current time resolution on the kinetic measurements is 10−20 ms. At higher temperatures where the signal is smaller and faster, the rate constants determined are less accurate. As a control, we also measured the temperature dependence of the decay from the photostationary state in solution. Some data at 460 nm obtained in 10 mM phosphate (pH 7.0) at several temperatures are shown in Figure 8b.

Figure 9a shows the effects of temperature on the rates of relaxation from the photostationary state in crystals. Both the fast and slow rate constants show similar temperature dependence. The results under two different solvent condi-

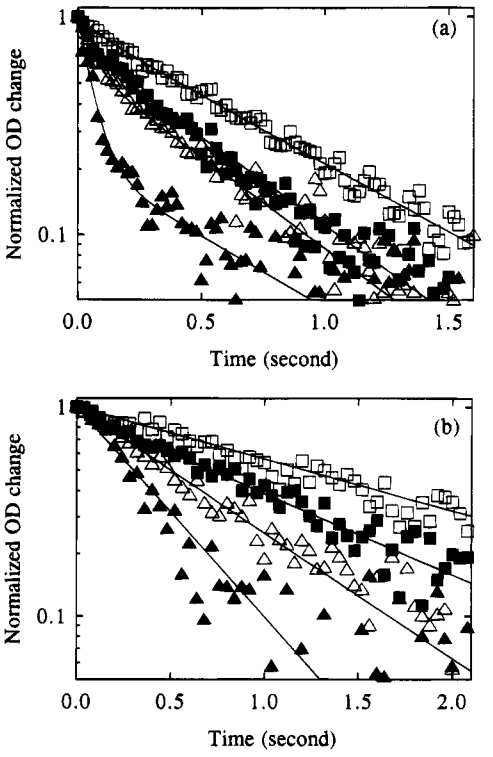

FIGURE 8: (a) Kinetics of relaxation from the photostationary state in PYP crystals after CW laser illumination at 496.5 nm for 200 ms measured at several temperatures: (▲) 7.0 °C; (△) 1.0 °C; (■) −2.3 °C and (□) −6.5 °C. The data points are measurements at 470 nm obtained from the time-resolved difference spectra. The solid lines are two exponential fit of the data. (b) Kinetics of relaxation from the photostationary state in PYP solution carried out in 10 mM phosphate and pH 7.0 under identical laser excitation conditions as in the case of crystals: (▲) 9.7 °C; (△) 3.8 °C; (■) −1.0 °C and (□) −5.8 °C. The solid lines are one exponetial fit of the data.

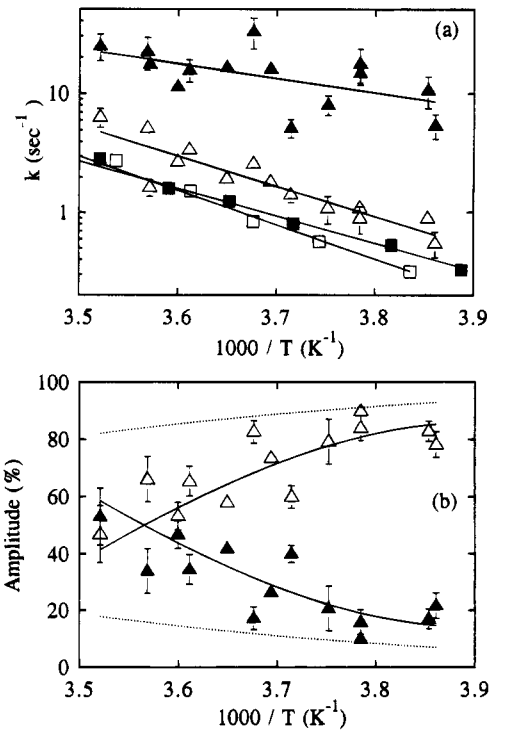

FIGURE 9: (a) Arrhenius plot of temperature effects on the relaxation kinetics from the photostationary state in PYP crystals after CW laser illumination at 496.5 nm for 200 ms. Global exponential fit of the data reveals biphasic kinetics: (▼) the faster components, (▽) the slower components. The solid lines are the least squares fit of the data to the Arrhenius equation. Also shown are Arrhenius plot of temperature effects on the kinetics of relaxation from the photostationary state in PYP solution under identical laser excitation conditions as in the case of crystals: (□) measurements carried out in 10 mM phosphate (pH = 7.0); (■) measurements carried out in 50% saturated ammonium sulfate. The two sets of solution data are fitted separately to the Arrhenius equation. (b) Plot of the relative amplitudes associated with the the two exponential components as a function of temperature, with the same symbols for the fast and slow components respectively as in a. The solid lines are regression lines drawn through the data points. Also shown is the predicted temperature effects on the relative amplitudes of ΔOD for the two components in PYP crystals (dashed lines). These amplitudes are calculated using the fitted temperature dependence of the two observed rate constants and the kinetic model 1 as described in the Discussion.

tions, namely 10 mM phosphate, pH 7, and 50% saturated ammonium sulfate, are also shown in Figure 9a. The 50% saturated ammonium sulfate case was chosen to resemble the crystallization conditions. The rate constants for both solvent conditions are very similar at all temperatures. Their temperature dependences are also very similar and follow normal Arrhenius behavior (Figure 9a). The activation energy calculated in 10 mM phosphate is 13.2 ± 0.7 kcal/mol and that in 50% saturated ammonium sulfate is 10.6 ± 0.5 kcal/mol. These values are about two times higher than that obtained for the recovery reaction, I_2 to P, using pulsed laser excitation (Meyer et al., 1989). It is also clear from Figure 9a that the rate constants for both the fast and slow components observed in the crystal show a temperature dependence very similar to that in solution. The calculated activation energies for the slow and fast components in the crystal are 11.7 ± 1.2 and 5.5 ± 2.3 kcal/mol, respectively. However, the relative amplitudes of the two exponents in the case of crystal vary with temperature in the opposite direction (Figure 9b). For the temperature range from 7 °C to −15 °C, the relative amplitude for the fast phase decreases from about 50% to less than 20%, whereas the relative amplitude for the slow phase increases from about 50% to greater than 80%.

We conclude that the intermolecular contacts in the crystal lattice, but not the very different solvent conditions required for crystallization, have a significant effect on the kinetics. A monophasic decay in solution is replaced by a biphasic decay in the crystal, which suggests that the kinetic model obtained from solution studies is not entirely adequate to describe the behavior of the crystal.

On-Line Optical Experiment. We have also carried out the optical experiments in parallel with X-ray data collection on beamline X-26C (Getzoff et al., 1993) at the National Synchrotron Light Source during a synchrotron run in June 1993. The measurements were made at −4 °C. Table 1 shows the mean kinetic fitting results from the seven crystals used during this synchrotron run. The multiwavelength analysis gave 2 exponential components with similar rate constants, 1.4 ± 0.2 and 5.2 ± 0.9 s^{-1}. The slower component accounts for about 60% of the total OD change and the faster, the other 40%. This is consistent with the off-line subsidiary measurements made in the laboratory.

DISCUSSION

Solution studies of PYP have been interpreted in terms of unidirectional photocycle kinetics, in which each step is characterized by a single rate constant (Figure 1; Meyer et

al., 1987). However, our studies with PYP crystals on the relaxation from the photostationary state show biphasic kinetics at some temperatures. Since there is only one molecule per asymmetric unit in the crystal, all molecules have the same environment. The biphasic kinetics cannot be due to two populations of molecules with different environments in the crystal lattice. The temperature dependence of the two rate constants is similar but that of the amplitudes is different and opposite. In order to interpret these data, we need to extend the solution model for the photocycle to apply to the crystals.

A major goal of reaction monitoring in crystals by optical means is to establish the presence of activity and the kinetics of interconversion of spectroscopically distinguishable species in quantitative terms. A kinetic model consistent with the optical data obtained in crystals is important in extracting the underlying structural intermediates from the X-ray diffraction data. In a time-resolved experiment, the populations of various molecular conformations vary with time. This gives rise to the variation with time of both the absorption spectrum in optical monitoring and the X-ray diffraction intensities, which arise from a time average over all molecular conformations that exist during the X-ray exposure and from a volume average over all molecules illuminated. However, we emphasize that there is no a priori relation between the X-ray and optical data. In the simplest model, the time variation of the absorbance change exactly parallels the time variation of diffraction intensities. This means that both the absorption spectrum from optical monitoring and the diffraction intensities from X-ray monitoring vary with time as a sum of exponentials and the exponents are identical in both. However, the amplitudes of the exponents for optical and X-ray data may not be correlated. Intermediates of low fractional occupancies but with high difference extinction coefficients, or those with high fractional occupancies but with low difference extinction coefficients, can give rise to similar absorbance changes but very different diffraction intensity differences. In the extreme case where a structurally different but optically silent (that is, no change in extinction coefficients) intermediate exists during the reaction, it is not directly detected by optical monitoring but by X-ray monitoring only and vice versa. The observed time-dependent average structural amplitudes arise from the time variation of the fractional populations of the several structural components, each with individual, time-invariant structural amplitudes (Moffat, 1989). These individual structure amplitudes may be extracted provided the kinetics of interconversion of the various species in the model, and hence their fractional populations at all times are known. Although the precise time course may in principle be derived from the variation of the diffraction intensities, a very large amount of data at numerous time points would have to be collected. In practice, an initial model may be more accurately derived from the optical data and tested for consistency with the X-ray data.

No unique kinetic model can ever account for kinetic data. The challenge is to rule out certain plausible models inconsistent with the data, and to identify other consistent, promising model(s). A powerful constraint is that, for all models which describe decay from a photostationary state, there is a mathematical relationship between the relative amplitudes and the magnitudes of the exponents. We take the solution model as the starting point and consider various simple modifications to it to account for our kinetic data on crystals. All models assume that P → P* is the only light-driven step of the photocycle.

Scheme 1

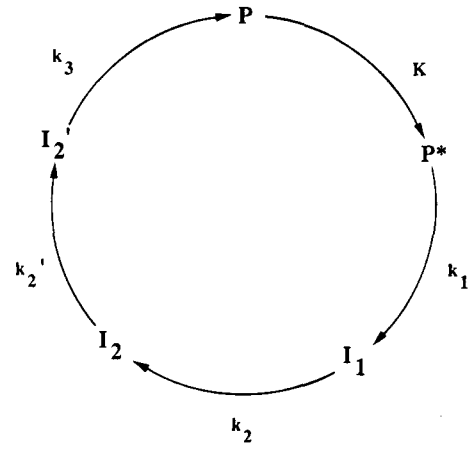

There are some characteristic features of the solution model, and all sequential models derived from it. The last intermediate has the longest lifetime and thus controls the lifetime of the photocycle. If there are N kinetic species (including the ground state) with only one light-driven step and the species interconvert via first order reactions, then the time dependence of the last intermediate of the photocycle has $(N - 1)$ exponential terms (for example see eq 14, in which $I_2(t)$ has three exponential terms). The magnitudes of the exponents are related to the individual first order rate constants of each step. The ratio of these amplitudes can be approximated as follows with the assumption that $k_1 \gg k_2$, k_3:

$$\frac{A_2(I_2)}{A_3(I_2)} \approx \frac{k_3}{k_2} \tag{15}$$

The temperature dependence of the relative amplitudes is thus predicted to be identical to that of the ratio of the exponents. According to these models, the two exponents would have to be similar in magnitude in order to account for the relative amplitudes observed at higher temperatures, contrary to our results. The fitted temperature dependence for the two exponents, as shown in Figure 9a, would predict a modest temperature effect of only about 10% on the amplitudes, less than observed (Figure 9b). Again, this is contrary to our observation. Clearly, the solution model does not apply to the crystal.

The solution model (Figure 1) can be extended by adding another sequential bleached intermediate (Scheme 1). This is the original model proposed for the PYP photocycle kinetics (Meyer et al., 1987). The relaxation time course of I_2 now has three exponential terms (k_1, k_2, and k_2') whereas that of I_2' has an extra term (k_3). If $k_2' \ll k_3$ and I_2 is the longest lived intermediate, the relaxation kinetics from the photostationary state is identical to that described above. On the other hand, if $k_2' \gg k_3$, the relaxation kinetics are mainly due to I_2'. Thus, using the above arguments, this extended sequential model provides similar predictions for the relative amplitudes and their temperature dependencies, which again are inconsistent with our data. This model too fails.

Another possibility is to add a branching reaction to the solution model, for example, a direct reaction from I_1 back

Scheme 2

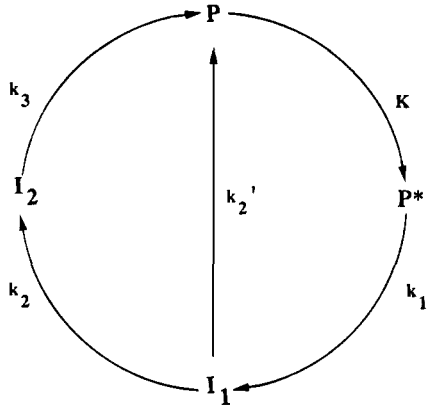

Scheme 3

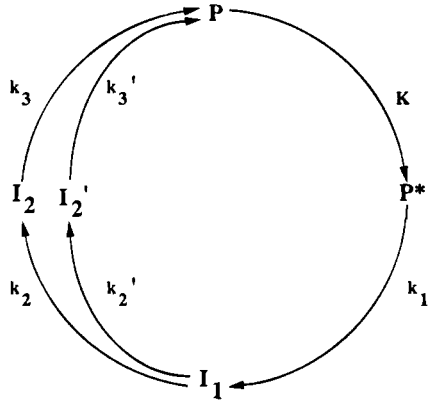

to P with a rate constant of k_2' (Scheme 2). Equations 14 are also applicable in this case, with k_2 replaced by $K_2 = k_2 + k_2'$. If $k_2 \ll k_3$, then $[I_2] \ll [I_1]$ in the photostationary state and the relaxation is predominantly from I_1 with a rate constant of K_2, which is basically monophasic. On the other hand, if $k_2 \gg k_3$, the relaxation kinetics from the photostationary state are mainly due to I_2 (with the continued assumption that k_1 is much larger than all the other k_i's). The relative amplitudes associated with K_2 and k_3 for $[I_2]$ or $\Delta OD(I_2)$ can be shown to be equal to k_3/K_2 using the same arguments as above. Again, this model fails. However, a direct shunt reaction induced by illumination at 366 nm in the near UV has been proposed for PYP in solution (Miller et al., 1993). There is no evidence that this reaction can be driven by excitation at wavelengths on the red side of the ground state absorption peak, for example at 496.5 nm, the excitation wavelength used for all our experiments.

The "bleached" intermediate can also be added to the photocycle in a parallel pathway (Scheme 3). Both I_2 and I_2' can relax to P and contribute to the observed kinetics. The time courses of absorbance change for both I_2 and I_2' back to P have three exponentials, (k_1, K_2, and k_3) and (k_1, K_2, and k_3'), respectively, where $K_2 = k_2 + k_2'$. The relative concentrations of $[I_2']$ and $[I_2]$ in the photostationary state are

$$\frac{[I_2']}{[I_2]} = \frac{k_2'}{k_2}\frac{k_3}{k_3'}$$

If k_2 and k_2' are very different in magnitude, then either I_2or I_2' is the dominant species in the photostationary state and the kinetics are monophasic with rate constant k_3 or k_3'. On the other hand, if k_2 and k_2' are similar, then the kinetics will appear to be biphasic. Further, the observed kinetics can switch from one branch to the other if the formation and decay of I_2 and I_2' depend differently on temperature. Confirmation of this promising model, which is consistent with all our data, requires further study of the kinetics of the buildup of the photostationary state and its temperature dependence.

By carefully selecting conditions for continuous laser excitation, we have initiated the photocycle in PYP crystals and established a saturated photostationary state. The relaxation from the photostationary state is found to be biphasic at some temperatures, which is inconsistent with the solution model but consistent with a modification of that model with two parallel pathways from I_1 back to the ground state P. A novel aspect of this work is that the optical monitoring is carried out on crystals that are also used for X-ray diffraction data collection. This is highly desirable, but the experimental requirements are very different for the X-ray and the optical monitoring. We have shown that, by paying careful attention to the optical properties of the crystals and to the photochemistry of the reaction initiation, these requirements can be met and artifacts can be minimized.

ACKNOWLEDGMENT

We thank Gloria E. O. Borgstahl, DeWight R. Williams, Patrick M. Burke, and Che-Fu Kuo for protein purification and crystallization and for providing all the crystals and protein solution used in this study, Michael Garavito, Daniel Picot, and Marvin Makinen for initial help with linear dichroism measurements, Ying Chen, Alan LeGrand, and Vukica Srajer for help with the microspectrophotometer, Claude Pradervand for help on timing and electronics components, Ying Chen, Alan LeGrand, Duncan McRee, Vukica Srajer, and Tsu-yi Teng for many helpful discussions, and Eric Gouaux and Marvin Makinen for comments on the manuscript.

REFERENCES

Baca, M., Borgstahl, G. E. O., Boissinot, M., Burke, P. M., Williams, D. R., Slater, K. A., & Getzoff, E. D. (1994) *Biochemistry 33*, 14369−14377.

Chen, Y. (1994) Ph.D. Dissertation, Cornell University.

Chen, Y., Srajer, V., Ng, K., LeGrand, A. D. & Moffat, K. (1994) *Rev. Sci. Instrum. 65*, 1506−1511.

Churg, A. K., & Makinen, M. W. (1978) *J. Chem. Phys. 68*, 1913−1925.

Cruickshank, D. W. J., Helliwell, J. R., & Johnson, L. N. (1992) *Philos. Trans. Roy. Soc. London A 340*, 167−334.

Cruickshank, D. W. J., Helliwell, J. R., & Moffat, K. (1991) *Acta Crystallogr. A47*, 352−373.

Getzoff, E. D., Jones, K. W., McRee, D., Moffat, K., Ng, K., Rivers, M. L., Schildkamp, W., Singer, P. T., Spanne, P., Sweet, R. M., Teng, T.-Y., & Westbrook, E. M. (1993) *Nucl. Instrum. Methods Phys. Res. B79*, 249−255.

Hajdu, J., & Andersson, I. (1993) *Annu. Rev. Biophys. Biomol. Struct. 22*, 467−498.

Hajdu, J., Machin, P. A., Campbell, J. W., Greenhough, T. J., Clifton, I. J., Zurek, S., Gover, S., Johnson, L. N., & Elder, M. (1987) *Nature (London) 329*, 178−181.

Makinen, M. W., & Fink, A. L. (1977) *Annu. Rev. Biophys. Bioeng. 6*, 301−343.

McRee, D. E., Meyer, T. E., Cusanovich, M. A., Parge, H. E., & Getzoff, E. D. (1986) *J. Biol. Chem. 261*, 13850−13851.

McRee, D. E., Tainer, J. A., Meyer, T. E., Van Beeumen, J., Cusanovich, M. A., & Getzoff, E. D. (1989) *Proc. Natl. Acad. Sci. U.S.A. 86*, 6533−6537.

Meyer, T. E. (1985) *Biochim. Biophys. Acta 806*, 175−183.

Meyer, T. E., Yakali, E., Cusanovich, M. A., & Tollin, G. (1987) *Biochemistry 26*, 418−423.

Meyer, T. E., Tollin, G., Hazzard, J. H., & Cusanovich, M. A. (1989) *Biophys. J. 56*, 559−564.

Meyer, T. E., Tollin, G., Causgrove, T. P., Cheng, P., & Blankenship, R. E. (1991) *Biophys. J. 59*, 988−991.

Meyer, T. E., Cusanovich, M. A., and Tollin, G. (1993) *Arch. Biochim. Biophys. 306*, 515−517.

Miller, A., Leigeber, H., Hoff, W. D., & Hellingwerf, K. H. (1993) *Biochim. Biophys. Acta 1141*, 190−196.

Moffat, K. (1989) *Annu. Rev. Biophys. Biophys. Chem. 18*, 309−332.

Moffat, K., Chen, Y., Ng, K., McRee, D., & Getzoff, E. D. (1992) *Philos. Trans. R. Soc. London A 340*, 175−190.

Mozzarelli, A., Rivetti, C., Rossi, G. L., Henry, E. R., & Eaton, W. A. (1991) *Nature (London) 351*, 416−419.

Schlichting, I., Almo, S. C., Rapp, G., Wilson, K., Petratos, K., Lentfer, A., Wittinghofer, A., Kabsch, W., Pai, E. F., Petsko, G. A., & Goody, R. S. (1990) *Nature (London) 345*, 309−315.

Singer, P. T., Smalas, A., Carty, R. P., Mangel, W. F., & Sweet, R. M. (1993) *Science 259*, 669−673.

Sprenger, W. W., Hoff, W. D., Armitage, J. P., & Hellingwerf, K. J. (1993) *J. Bacteriol. 175*, 3096−3104.

Van Beeumen, J. J., Devreese, B. V., Van Bun, S. M., Hoff, W. D., Hellingwerf, K. J., Meyer, T. E., McRee, D. E., & Cusanovich, M. A. (1993) *Protein Sci. 2*, 1114−1125.

Zelano, J. A., Sigountos, J. G., Makinen, M. W., and Sanders, H. (1985) *Rev. Sci. Instrum. 56*, 398−401.

BI9421580